ORION EXPLORATION FLIGHT TEST-1 (EFT-1) ABSOLUTE NAVIGATION PERFORMANCE

Renato Zanetti*

INTRODUCTION

The Orion vehicle, being design to take men back to the Moon and beyond, successfully completed its first flight test, EFT-1 (Exploration Flight Test-1), on December 5th, 2014. The main objective of the test was to demonstrate the capability of re-enter into the Earth's atmosphere and safely splash-down into the pacific ocean. This un-crewed mission completes two orbits around Earth, the second of which is highly elliptical with an apogee of approximately 5908 km, higher than any vehicle designed for humans has been since the Apollo program. The trajectory was designed in order to test a high-energy re-entry similar to those crews will undergo during lunar missions. The mission overview is shown in Figure 1.

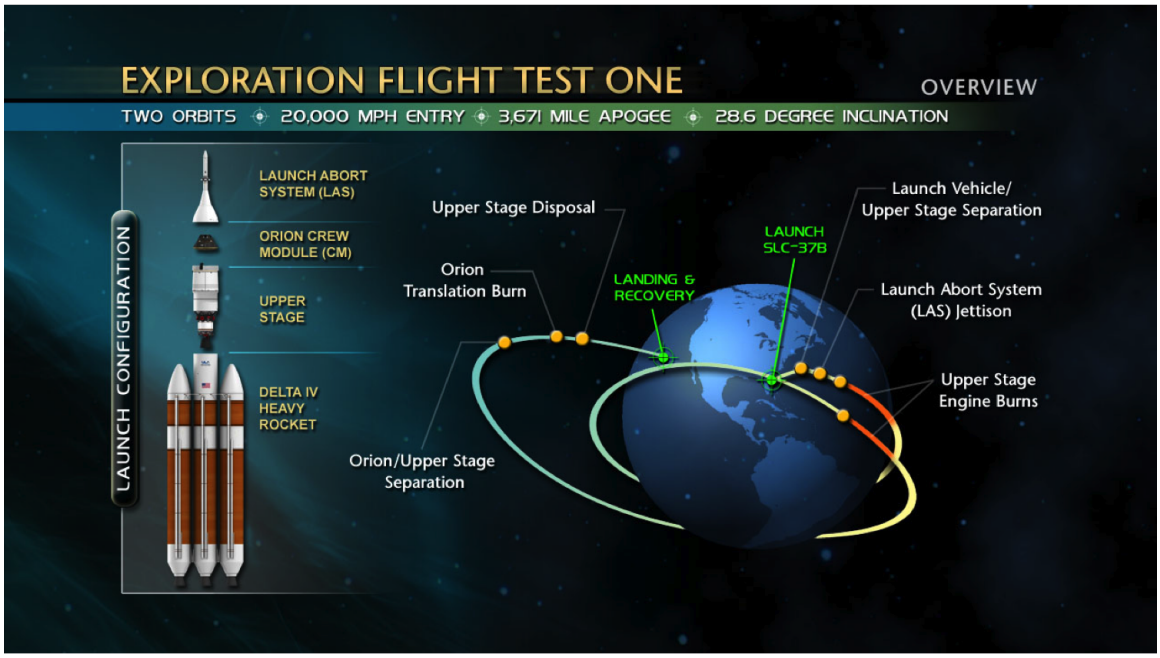

Figure 1. EFT-1 Mission Profile

*GN&C Autonomous Flight Systems Engineer, Aeroscience and Flight Mechanics Division, EG6, 2101 NASA Parkway. NASA Johnson Space Center, Houston, Texas 77058.

The objective of this paper is to document the performance of the absolute navigation system during EFT-1 and to present its design.

ABSOLUTE NAVIGATION DESIGN

This section briefly repeats the design of the Orion EFT-1 absolute navigation design as described in Refs. [1] and [2].

Two Orion Inertial Measurement Units (OIMUs), a GPS receiver (GPSR) and three barometric altimeters (BALTs) comprise the Orion sensor suite. The OIMUs provide integrated accelerometer and gyro data at high rate. The inertial state is propagated at 40Hz and is updated by GPSR pseudorange (PR) and deltarange (DR) measurements at 1Hz. The attitude of the vehicle is initialized by gyro-compassing, is updated with integrated velocity (IV) measurements while on the pad, and is updated with GPSR measurement when available during flight.

The BALTs measurements are not incorporated into the navigation filter, but they are used as back ups by the Navigation Fault Detection, Isolation, and Recovery algorithm (FDIR). In the event the GPSR fails or if the filtered solution has diverged, the FDIR logic autonomously selects the BALT output as the primary source of altitude. The logic accomplishes this by comparing the EKF covariance in the radial direction with a parameterized threshold value. FDIR also checks the filter's performance by monitoring the measurements' acceptances and rejections.

Each of the flight computers contains two instances of the navigation filter, each slaved to a different OIMU. The purpose of this design is to allow for an instantaneous recovery after an OIMU failure without having to go to a transient period to estimate the OIMU error states or for the filter to re-converge. Each OIMU is tied to a navigation channel, each channel contains several Computer Software Units (CSUs): an IMU Sensor Operating Procedure (IMUSOP) that is responsible for parsing the OIMU data, a Coarse Align (CAlign) CSU that is responsible for providing a crude estimate of the initial attitude on the pad, a Filtered Navigator (FILTNAV) CSU that is responsible for multiplexing the OIMU data with the GPS updates and an Inertial Navigator (INRTLNAV) CSU that is responsible for maintaining an un-aided (OIMU-only) state. INRTLNAV and FILTNAV have counterparts on the 1Hz side. The Inertial Navigator Gravity (InrtlNavGrav) and Extended Kalman Filter (EKF) CSUs on the 1Hz side provide a higher-order gravity estimate to INRTLNAV and state updates to FILTNAV, respectively.

The outputs of the two channels are received by Navigation FDIR (NAVFDIR) CSU which selects the primary state. The NAVFDIR scheme relies on the IMUFDIR outputs and performs additional tests on the filtered solution. One of the checks it relies on is the percentage of PR/DR measurements being accepted by each channel.

Prior to launch the filter is initialized with the coarse align attitude and an inertial position derived from the current time and the coordinates of the pad. This pre-launch navigation phase is called fine align and the only measurement active in this mode is integrated velocity, which is a pseudo-measurement consisting of a zero change of Earth-referenced position over a 1 second interval. The GPSR measurement are not available during fine align. The main purpose of fine align is to better estimate the attitude and the IMU states.

The ascent phase is divided in two parts, the first when GPSR measurements are not enabled, and the second when they are. The only difference between Fine Align and Ascent Without GPS is that IV measurement processing flag is set to zero in the latter. The maximum number of processable measurements is set to 12 which is a large enough number to obtain very good performance while

keeping the throughput reasonably low. To avoid possible transient issues the first PR measurement is not processed. After a long blackout the covariance becomes very large and the nonlinearity of the DR measurement creates convergence issues. Through numerical simulation it was determined that allowing for multiple PR ($\sim$30s) to be processed before incorporating a DR mitigates this issue because the PRs shrink the uncertainty before DRs are introduced. If a satellite is not present for a single cycle, the counters are not reset and if the satellite comes back is immediately used as a measurement. If the satellite is absent for more than a cycle the counters are reset.

While it is allowed for the usage of the PR variance output from the GPS receiver, the EKF has a PR variance floor that will almost always prevent it from using the GPS receiver output value except in the case of very large values. Underweighting is applied when the estimated measurement has an uncertainty greater than $100ft$. One of the EFT-1 mission goals was to test GPSR clock stability, clock filter state restarts, and high altitude GPS processing.

GPSR measurements are processed throughout the orbit phase and during entry when available. A GPS blackout was expected and experienced during entry. In order to process latent GPS measurements the EKF necessitates to back-propagate its current state estimate to the measurement time. This task is made possible by a 4Hz buffer of OIMU data provided to EKF by FILTNAV. When accelerating fast under the chutes during entry, the attitude dynamics is not accurately represented by the 4Hz IMU buffer. Therefore PR and DR are inhibited above a certain angular velocity.

PRE-LAUNCH PERFORMANCE

During fine align the navigation filter process integrated velocity (IV) measurements. Figure 2 shows the performance of the filter processing this measurement by means of the measurement residual (actual measurement minus estimated measurement, blue lines) and their predicted covariance (red lines). It can be seen that the residuals are well within their predicted variance, all of the measurements are accepted (green line) and zero rejections occur (red line). The residuals are extremely small with respect to their predicted standard deviation, this suggests the filter is overly conservative. This fact was expected and a design choice to add robustness to large twist and sway motion of the launch vehicle. During the day of flight little to no twist and sway was observed. Figure 2 shows the results from Channel 1. a zoomed in plot of the residuals fro Channel 2 is shown in Figure 3. Throughout the flight the performance of the two channels is nearly identical, therefore only results from Channel 1 are shown for the remainder of this paper.

Figure 4 show the filter's position, velocity, and attitude covariance. Figures 5 and 6 show the accelerometer and gyro error states covariance, respectively. Figures 7 and 8 show the filter's estimates of the accelerometer and gyro errors, respectively. The performance is as expected.

Finally Figures 9 to 11 show the position, velocity, and attitude estimates from the user parameters processor (UPP) which provided the outputs from channel 1.

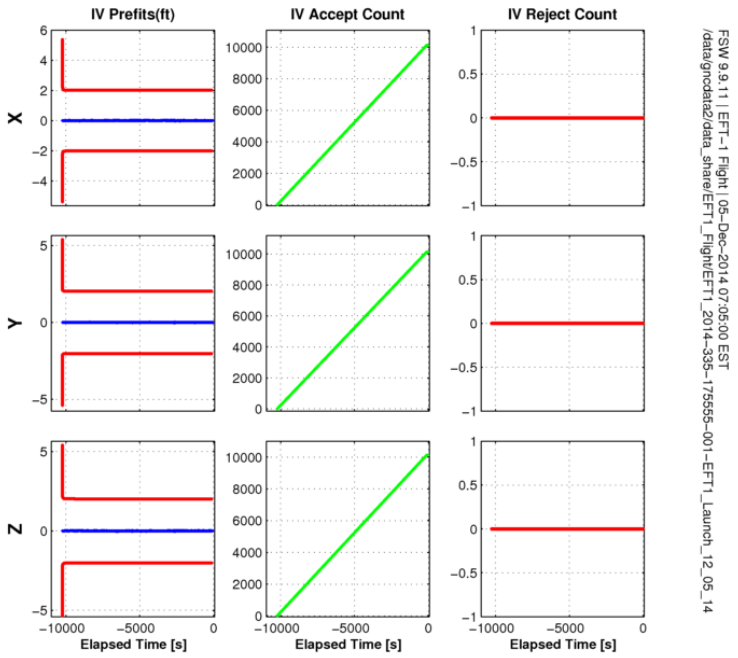

Figure 2. FCM1-CH1 IV Measurements

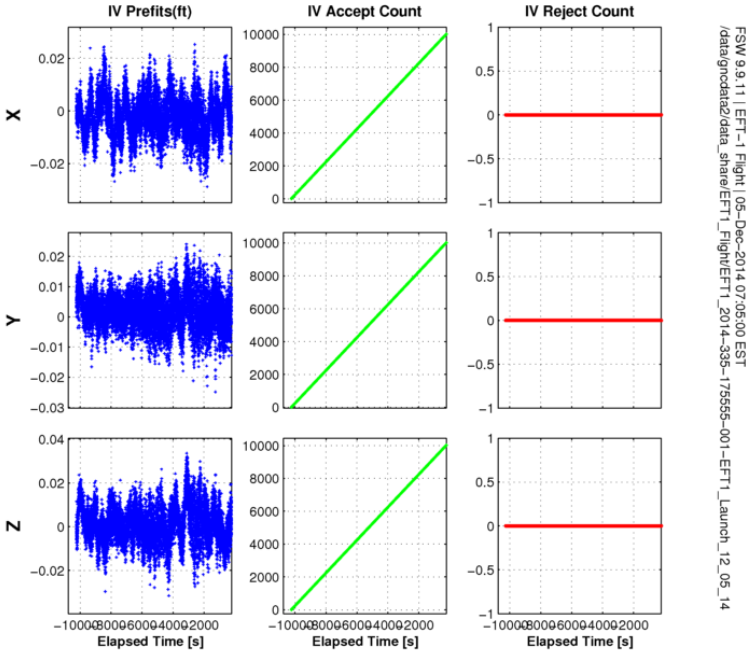

Figure 3. FCM1-CH2 IV Measurements

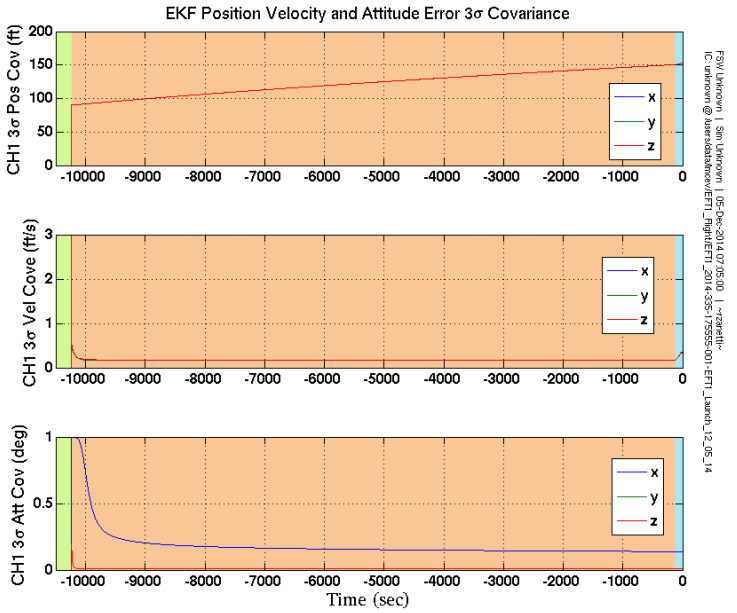

Figure 4. FCM1-CH1 Position, Velocity, and Attitude 3σ Covariance

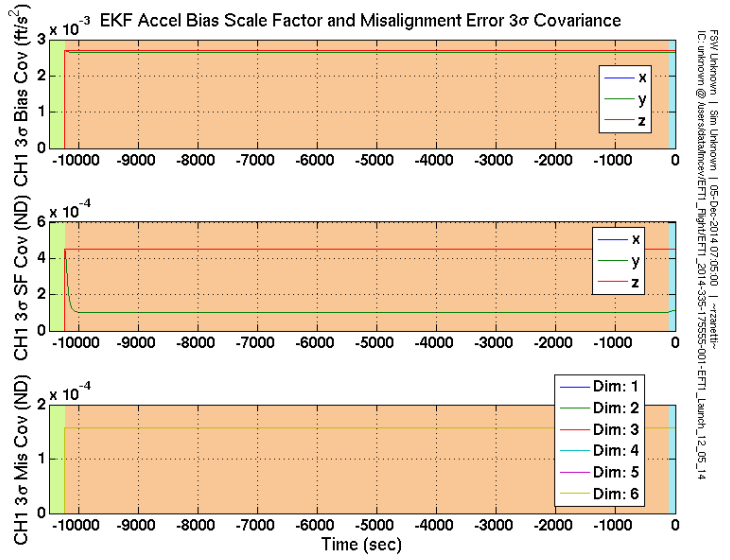

Figure 5. FCM1-CH1 Accelerometer Bias, Scale Factor, and Misalignment 3σ Covariance

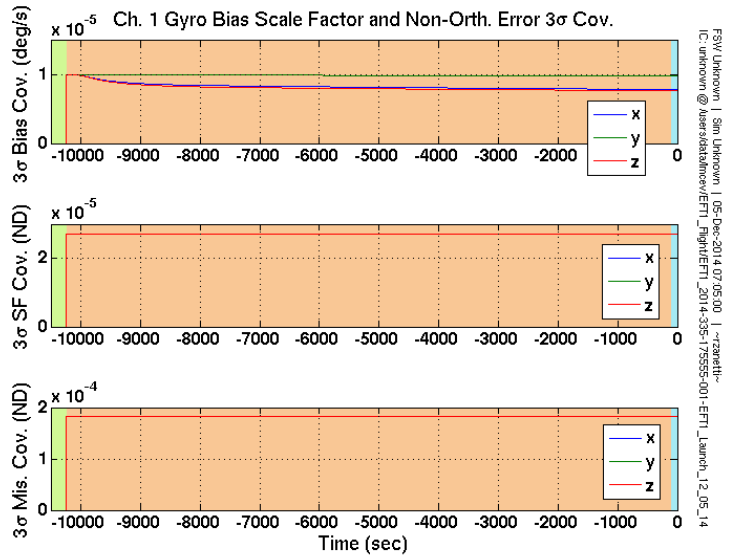

Figure 6. FCM1-CH1 Gyro Bias, Scale Factor, and Non-Orthogonality 3σ Covariance

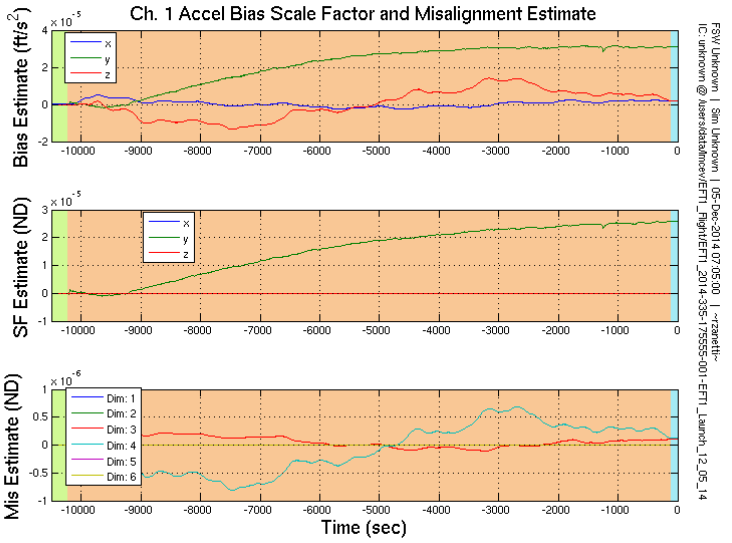

Figure 7. FCM1-CH1 Accelerometer Bias, Scale Factor, and Misalignment Estimate

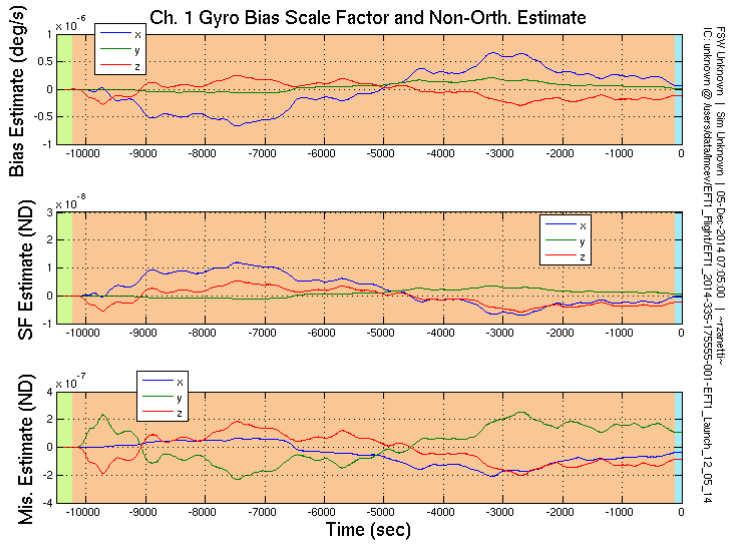

Figure 8. FCM1-CH1 Gyro Bias, Scale Factor, and Non-Orthogonality Estimate

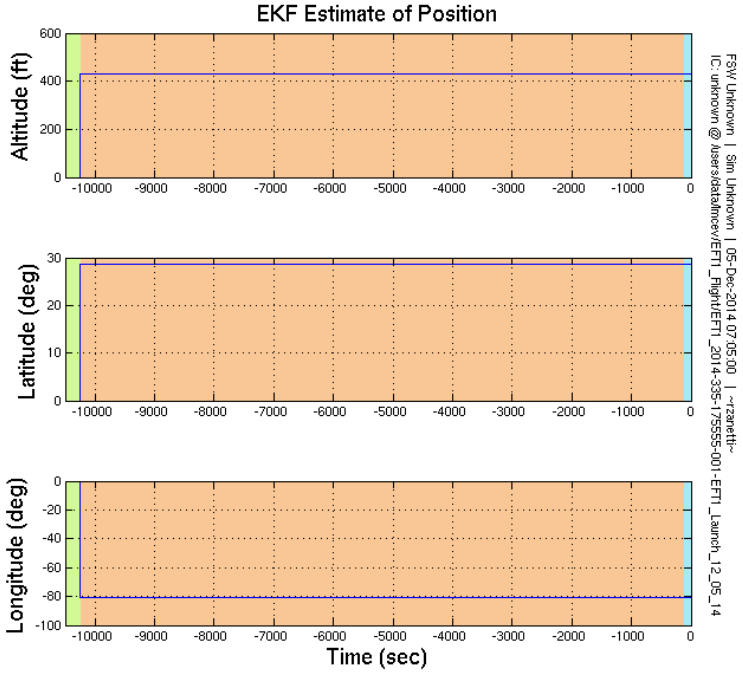

Figure 9. FCM1-CH1 Position Estimate

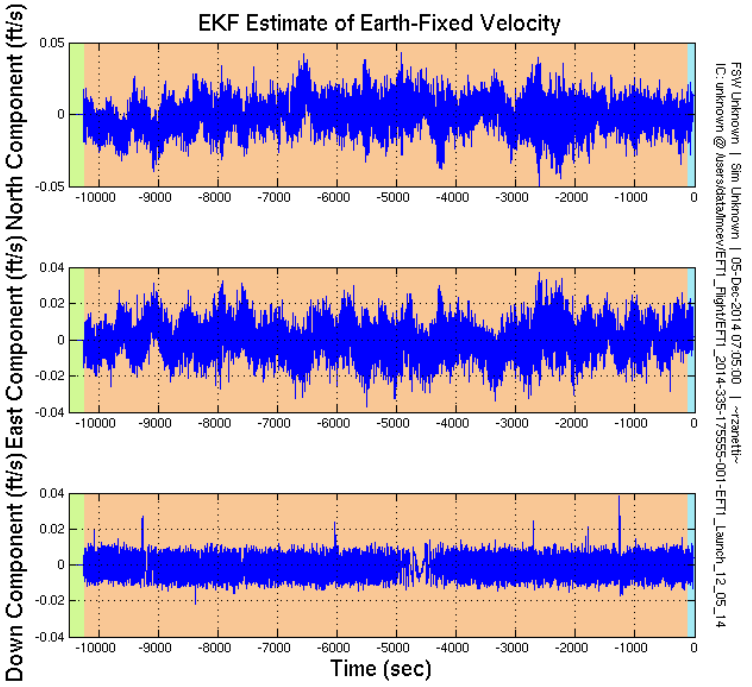

Figure 10. FCM1-CH1 Velocity Estimate

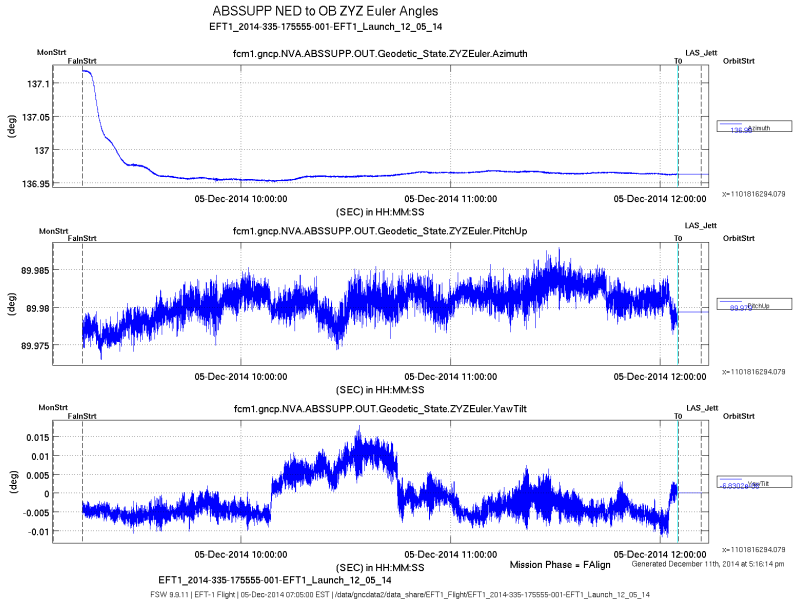

Figure 11. FCM1-CH1 Attitude Estimate

POST-LAUNCH PERFORMANCE

Figure 12 shows good EKF position covariance behavior throughout the flight. The estimates are typically bounded withing 50 ft (3σ) during coasting flight, and exhibit nominal growth and reconvergence during the brief outage caused by the CMsep attitude.

Figure 13 shows good EKF velocity covariance behavior throughout the flight. The estimates are typically bounded withing 0.3 ft/s (3σ) during coasting flight, and exhibit nominal growth and reconvergence during the second stage burn and the brief outage caused by the CMsep attitude.

Figure 14 shows good EKF attitude covariance behavior throughout the flight. The estimates are typically bounded withing 0.04 deg (3σ) during coasting flight, and converge lower during observable periods such as the second stage burn and entry.

Figure 15 shows good EKF clock bias covariance behavior throughout the flight. The estimates are typically bounded withing 50 ft (3σ) during coasting flight, and exhibit nominal growth and reconvergence during the brief outage caused by the CMsep attitude.

Figure 16 shows good EKF clock drift covariance behavior throughout the flight. The estimates are typically bounded withing 2 ft/s (3σ) during coasting flight, and exhibit nominal growth and reconvergence during the brief outage caused by the CMsep attitude.

Figure 17 shows EKF pseudorange counters with no rejected measurements for the entire flight.

Figure 18 shows EKF deltarange counters with no rejected measurements for the entire flight.

Figure 19 shows EKF pseudorange residuals. In general they are well behaved and bounded during the entire flight.

REFERENCES

[1] G. Holt, R. Zanetti, and C. D'Souza, "Tuning and Robustness Analysis for the Orion Absolute Navigation System," Presented at the 2013 Guidance, Navigation, and Control Conference, Boston, Massachusetts, August 19–22 2013. AIAA-2013-4876, doi: 10.2514/6.2013-4876.

[2] J. Sud, R. Gay, G. Holt, and R. Zanetti, "Orion Exploration Flight Test 1 (EFT1) Absolute Navigation Design," *Proceedings of the AAS Guidance and Control Conference*, Vol. 151 of *Advances in the Astronautical Sciences*, Breckenridge, CO, January 31–February 5, 2014 2014, pp. 499–509. AAS 14-092.

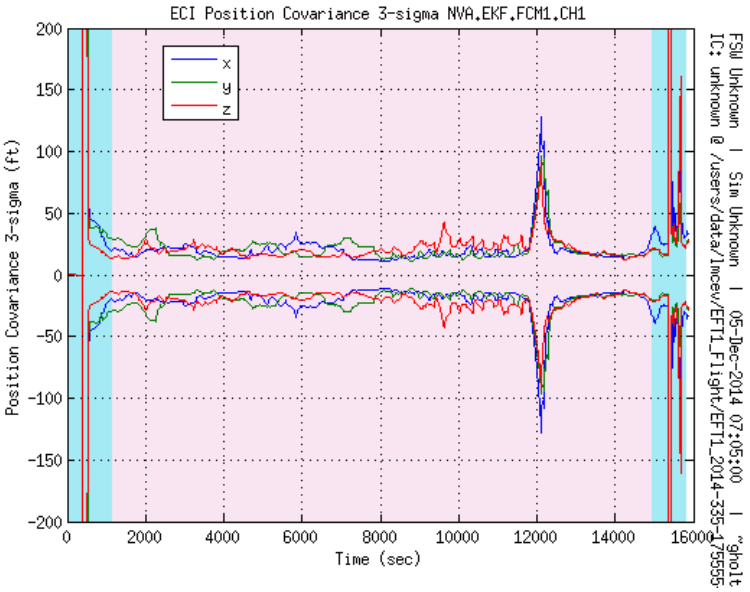

Figure 12. CH1 ECI Position Covariance 3σ

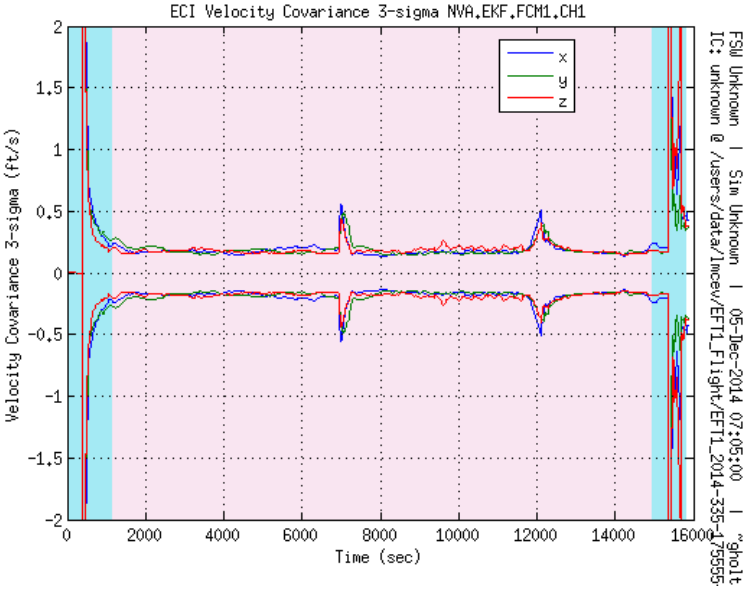

Figure 13. CH1 ECI Velocity Covariance 3σ

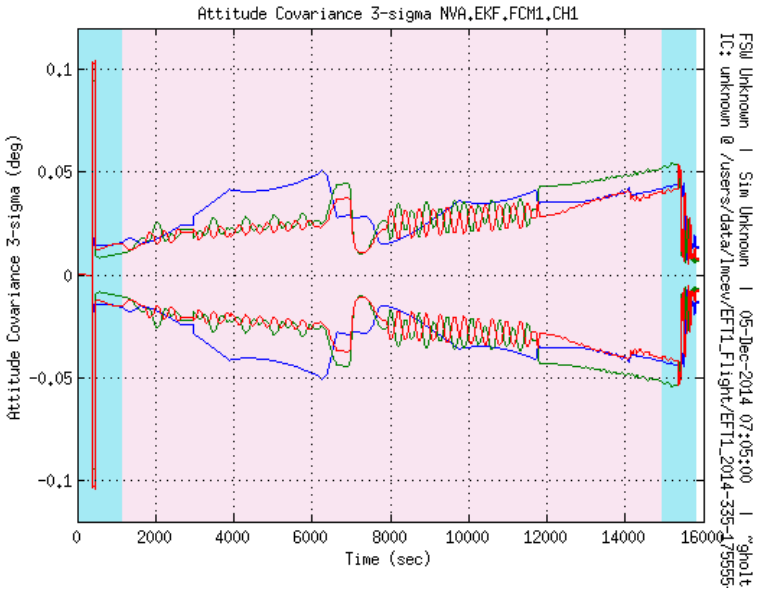

Figure 14. CH1 ECI Attitude Covariance 3σ

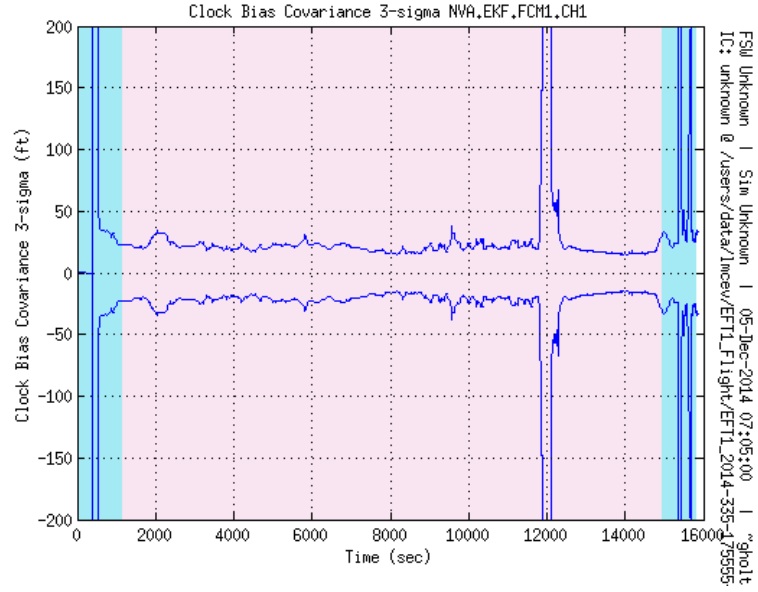

Figure 15. CH1 GPSR Clock Bias Covariance 3σ

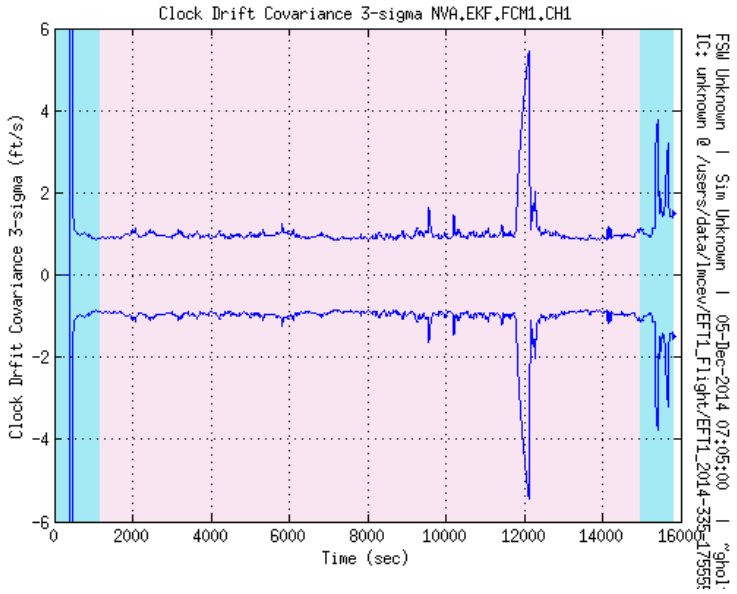

Figure 16. CH1 GPSR Clock Drift Covariance 3σ

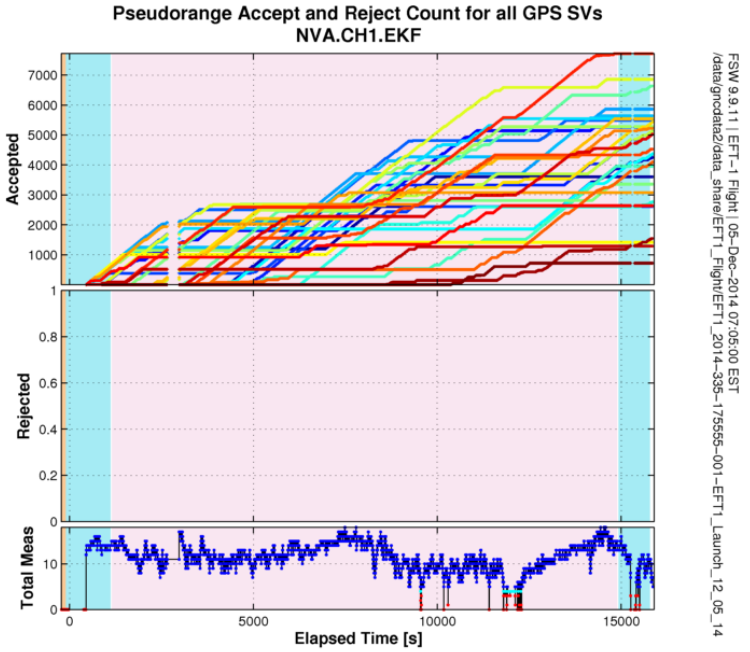

Figure 17. CH1 Pseudorange Counters

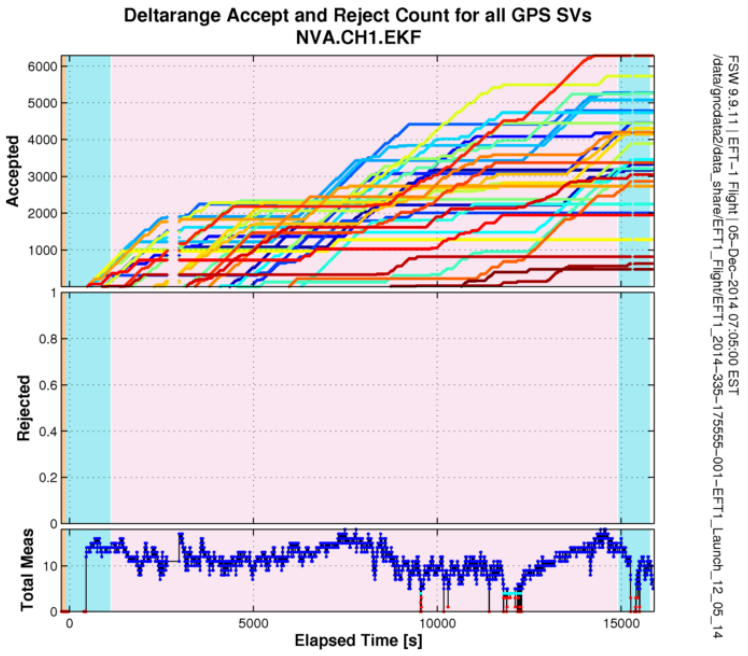

Figure 18. CH1 DeltaRange Counters

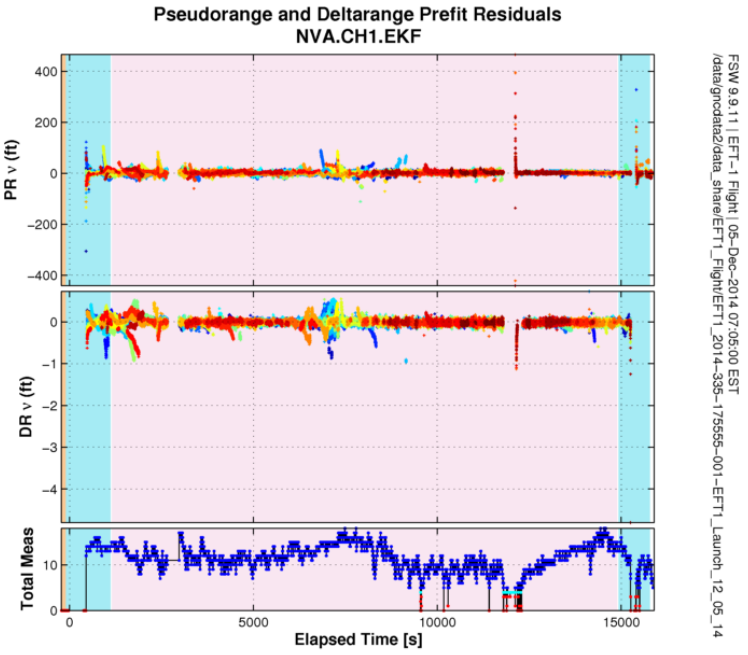

Figure 19. CH1 Pseudorange PreFit Residuals

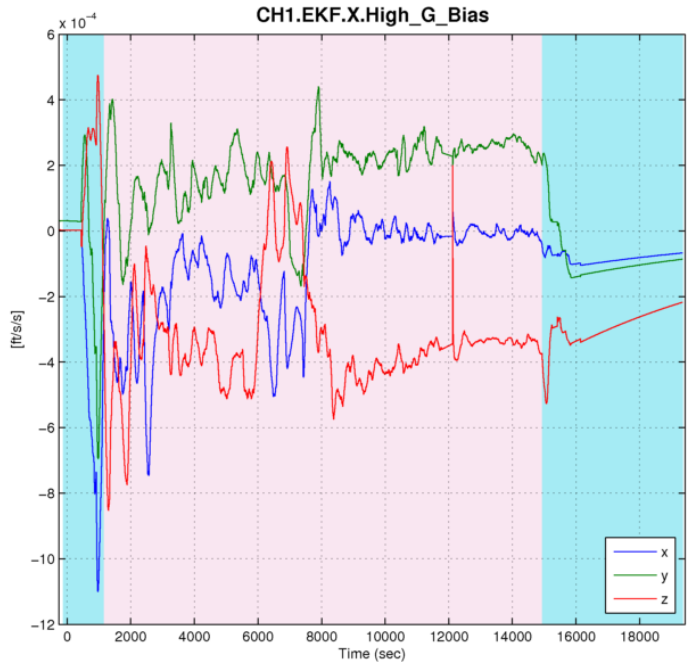

Figure 20. EKF CH1 Accel Bias (High-G)

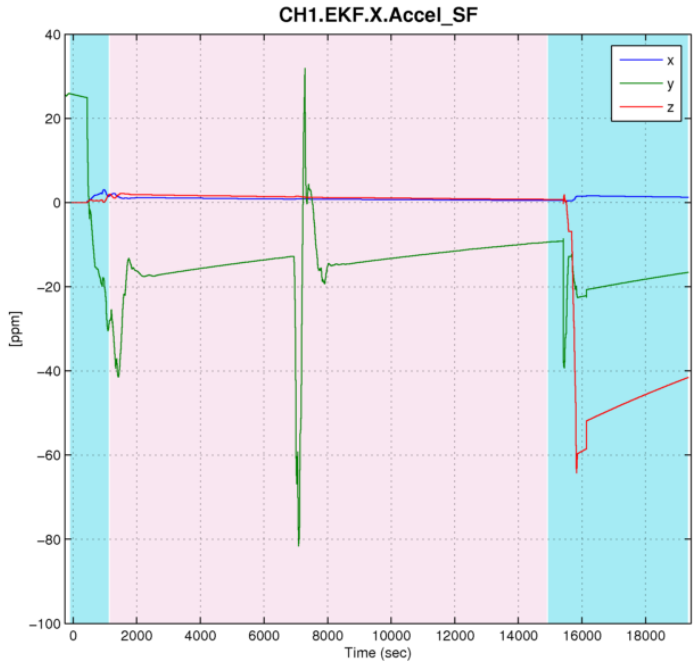

Figure 21. EKF CH1 Accel Scale Factor

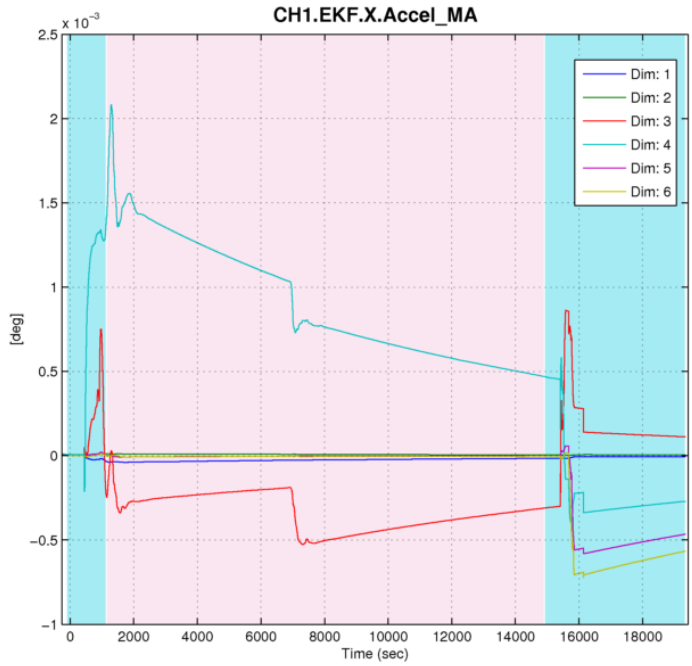

Figure 22. EKF CH1 Accel Misalignment States

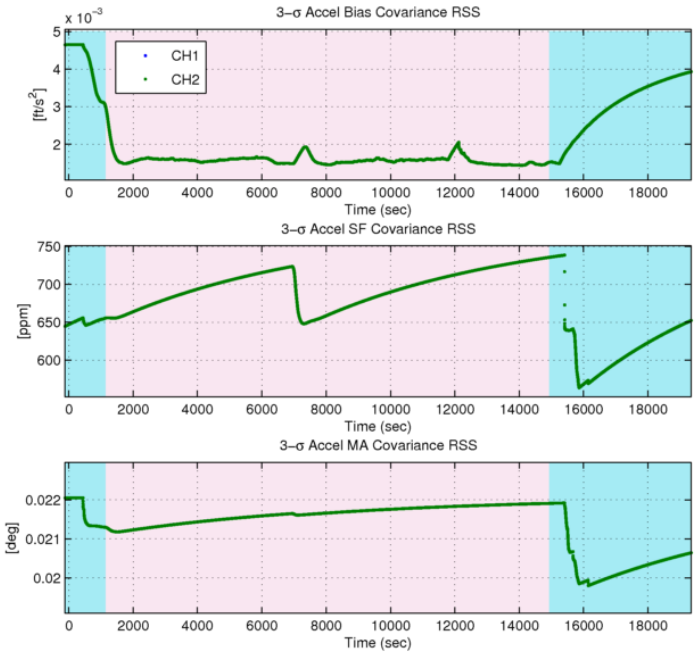

Figure 23. EKF CH1 Accel Rss 3-σ Covariance States

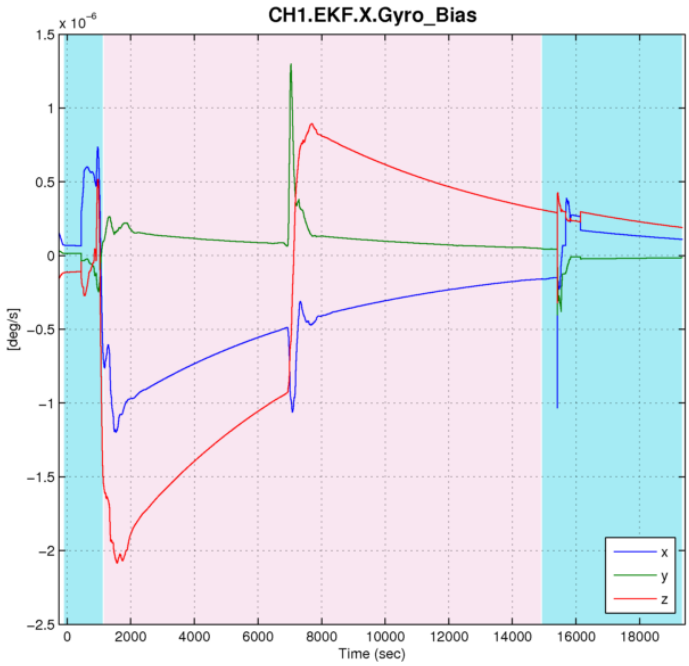

Figure 24. EKF CH1 Gyro Bias

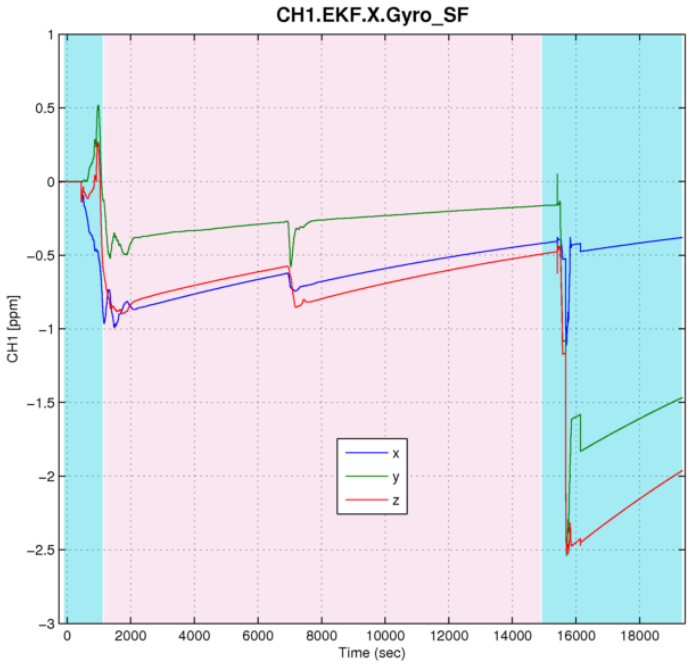

Figure 25. EKF CH1 Gyro Scale Factor

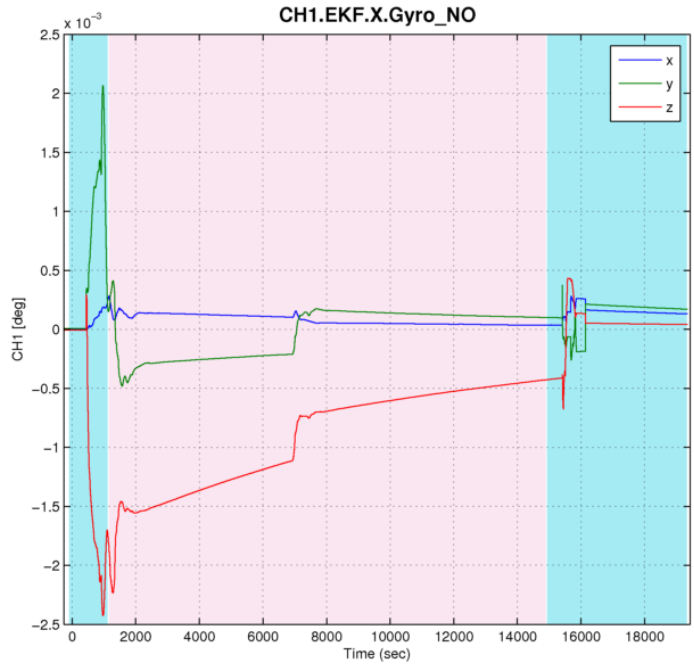

Figure 26. EKF CH1 Gyro Non-Orthogonality States

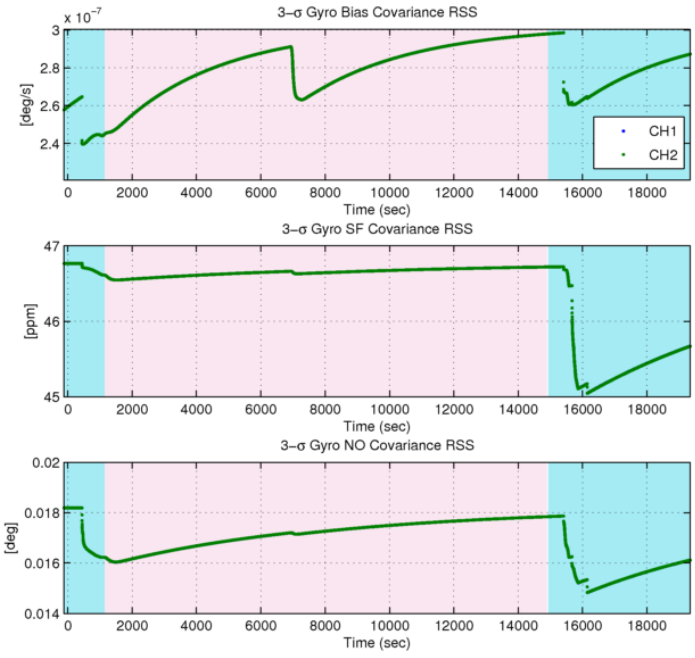

Figure 27. EKF CH1 Gyro Rss 3-σ Covariance States